TRANSPLANTATION

Allogeneic cell transplant expands bone marrow distribution by colonizing previously abandoned areas: an FDG PET/CT analysis

Francesco Fiz,[1] Cecilia Marini,[2] Cristina Campi,[3] Anna Maria Massone,[3] Marina Podestà,[4] Gianluca Bottoni,[1] Roberta Piva,[1] Francesca Bongioanni,[1] Andrea Bacigalupo,[5] Michele Piana,[6] Gianmario Sambuceti,[1] and Francesco Frassoni[5]

[1]Chair of Nuclear Medicine, Genoa University, Istituti di Ricovero e Cura e Carattere Scientifico San Martino Istituto Scientifico Tumori, Genoa, Italy; [2]Consiglio Nazionale delle Ricerche Institute of Molecular Bioimaging and Physiology, Milan, Section of Genoa, Genoa, Italy; [3]Consiglio Nazionale delle Ricerche SPIN (Superconductors, oxides and other innovative materials and devices), Genoa, Italy; [4]Department of Pediatric Hemato-Oncology, Stem Cell and Cell Therapy Laboratory, Istituto G. Gaslini, Genoa, Italy; [5]Hematology and Bone Marrow Transplantation Department, Istituti di Ricovero e Cura e Carattere Scientifico San Martino Istituto Scientifico Tumori, Genoa, Italy; and [6]Department of Mathematics, University of Genoa, Italy

Key Points

- Allogeneic hematopoietic stem cells colonize, other than axial niches, appendicular BM that is abandoned in normal subjects.
- Bone marrow expansion into distal sites differs between cord blood and adult hematopoietic stem cells.

Mechanisms of hematopoietic reconstitution after bone marrow (BM) transplantation remain largely unknown. We applied a computational quantification software application to hybrid 18F-fluorodeoxyglucose positron emission tomography (PET)/computed tomography (CT) images to assess activity and distribution of the hematopoietic system throughout the whole skeleton of recently transplanted patients. Thirty-four patients underwent PET/CT 30 days after either adult stem cell transplantation (allogeneic cell transplantation [ACT]; n = 18) or cord blood transplantation (CBT; n = 16). Our software automatically recognized compact bone volume and trabecular bone volume (IBV) in CT slices. Within IBV, coregistered PET data were extracted to identify the active BM (ABM) from the inactive tissue. Patients were compared with 34 matched controls chosen among a published normalcy database. Whole body ABM increased in ACT and CBT when compared with controls (12.4 ± 3 and 12.8 ± 6.8 vs 8.1 ± 2.6 mL/kg of ideal body weight [IBW], $P < .001$). In long bones, ABM increased three- and sixfold in CBT and ACT, respectively, compared with controls (0.9 ± 0.9 and 1.7 ± 2.5 vs 0.3 ± 0.3 mL/kg IBW, $P < .01$). These data document an unexpected distribution of transplanted BM into previously abandoned BM sites. (*Blood*. 2015;125(26):4095-4102)

Introduction

Current models of the adult hematopoietic function consider that active bone marrow (ABM) is homogeneously distributed within the intraosseous space of the whole axial skeleton, as well as in the hips and in the proximal epiphyses of humeri and femurs.[1] Accordingly, regardless of the sampling site, cellular and molecular analyses based on bone marrow (BM) aspiration or biopsy represent the standard for diagnosis, staging, and response assessment in the vast majority of blood disorders.[2] This notion implies that any modification of BM composition occurs almost synchronously in every BM district and that the circulation of a limited number of hematopoietic stem cells (HSCs) accounts for the tight adjustment of hematopoiesis to blood cell demand.

This physiological feature is a key mechanism of BM transplantation. Reconstitution of recipient hematopoietic function is possible with as little as 1% of donor BM, indicating a significant redundancy in the HSC reservoir in normal humans.[3] This small quota of donor BM can spread throughout the different skeletal segments and, following a considerable proliferative process, restore the host cell production and maintain the hematopoietic function indefinitely.[3]

Nevertheless, our limited knowledge about extension, distribution, and activity of transplanted BM cells in humans has prevented so far a full comprehension of determinants of its engraftment in various BM districts and its impact on transplantation outcomes.

The concept of even distribution of hematopoietic cell subsets has been recently challenged in the mouse model of BM transplant,[4] indicating that HSCs are not homogeneously distributed in the various BM areas. In addition, that study showed that granulocyte colony-stimulating factor (G-CSF) treatment plays a role in redistributing HSCs. On the other hand, the murine hematopoietic system significantly differs from human BM, as mice cannot possibly expand their hematopoietic system because their baseline blood elements production effort employs the whole BM as well as the spleen.[5] Conversely, in adult humans, only a proportion of BM spaces are occupied by functioning marrow.[1]

Some simple mathematical considerations might help to better define the importance of volumetric availability in the context of HSC turnover: overall, BM produces an average of 10^{11} granulocytes and 10^{11} erythrocytes per day.[6] Because volumes of these cells are 200 to 300 fL and 90 fL,[7,8] respectively, this activity roughly corresponds to a BM cell output averaging 30 to 50 mL per day. Considering a total BM asset of 10^{12} cells corresponding to 520 mL,[9,10] this would imply a cell renewal rate of 10% per day,

Submitted January 6, 2015; accepted April 30, 2015. Prepublished online as *Blood* First Edition paper, May 8, 2015; DOI 10.1182/blood-2015-01-618215.

The publication costs of this article were defrayed in part by page charge payment. Therefore, and solely to indicate this fact, this article is hereby marked "advertisement" in accordance with 18 USC section 1734.

Table 1. Characteristics of patients treated with CBT

Patient	Gender	Age (y)	Diagnosis	Platelets ($\times 10^9$/L)			Neutrophils ($\times 10^9$/L)			Axial ABM volume (ml/kg IBW)	Appendicular ABM volume (ml/kg IBW)	Disease status
				Day 30	Day 60	Day 100	Day 30	Day 60	Day 100			
1	M	63	NHL	10	16	54	0.1	3.4	2.6	6.00	2.68	PR
2	F	34	AML	10	33	19	1.5	7.8	5.3	4.5	0.05	CR
3	F	47	AML	15	73	115	3.8	3.0	4.3	4.4	0.11	CR
4	M	45	AML	30	99	125	0.6	2.0	5.4	3.32	2.23	CR
5	M	21	ALL	15	65	70	1.2	3.7	4.1	5.62	0.25	CR
6	M	44	AML	19	75	126	6.4	3.5	5.8	6.17	0.25	CR
7	M	35	ALL	70	212	54	6.3	2.7	19.6	5.63	0.49	CR
8	M	31	NHL	12	15	46	5.4	6.2	4.2	4.83	0.35	CR
9	F	30	MM	43	187	170	3.5	10.8	4.0	4.58	0.01	CR
10	M	49	ALL	14	90	129	1.5	3.8	2.6	6.49	0.79	CR
11	M	43	AML	19	81	97	1.0	2.5	1.8	4.19	0.26	CR
12	F	22	AML	41	144	97	3.2	7.2	3.4	4.99	2.04	CR
13	M	35	ALL	22	87	97	0.1	6.6	5.5	5.32	0.32	CR
14	M	53	AML	19	77	143	1.9	4.1	8.1	3.47	2 36	CR
15	M	56	AML	9	33	48	0.3	11.0	7.2	5.04	0.74	CR
16	M	46	MM	10	139	167	0.9	10.5	9.3	4.06	1.29	CR
Mean		41		23 ± 16	89 ± 57	98 ± 45	2.4 ± 2.1	5.6 ± 3.2	5.6 ± 4.4	4.9 ± 0.9	0.9 ± 0.9	15/16 CR
P vs ACT		NS		<.01	<.05	<.05	<.05	NS	NS	NS	<.05	NS

CR, complete response; F, female; M, male; NS, not significant; PR, partial response.

to account for the baseline physiological regenerative demand of adult subjects.

In the posttransplant setting, engrafted HSCs are required to undergo a tremendous proliferative effort to restore the normal blood elements values in the shortest possible time. The reconstitution *ad integrum* of the entire stem cell pool remains disputed, but this is beyond the scope and the possibilities of the present approach.[10,11] Restoration of normal hematopoiesis could be theoretically met using 2 different strategies. In the first scenario, HSCs could increase their proliferation rate within the standard active hematopoietic sites.[12] Alternatively, HSCs could recolonize intraosseous spaces that were abandoned because they were redundant for the standard homeostatic need, thus restoring the hematopoietic asset classically described in infancy.[13]

These 2 different patterns would imply divergent signaling mechanisms, whose relative contribution is yet undefined, because of the obvious concerns in performing repeated BM biopsies in multiple bone segments. Limited data are available on BM extension, distribution, and activity following HSC transplant, thus limiting our comprehension of the pathophysiological aspect of HSC engraftment and the impact of these parameters on the subsequent outcome. Such a limitation can be at least partially overcome by imaging approaches with positron emission tomography (PET)/computed tomography (CT) whose computational analysis has been shown to provide an accurate assessment of BM extension, distribution, and metabolic activity.[14-17]

In the present study, we applied this validated software tool to a series of patients[10] evaluated after IV adult BM transplantation (allogeneic cell transplantation [ACT]) or intrabone cord blood transplantation (CBT) to verify the homing features of transplanted HSCs.

Patients and methods

Patient populations

The study included 34 adult patients affected by different hematologic diseases, evaluated 1 month after transplant by whole body 18F-fluorodeoxyglucose (FDG)PET/CT scan. The study population comprised 23 males and 11 females, with an average age of 40 years (range, 17-65). Patients were referred to PET/CT evaluation for early assessment of treatment response or for suspicion of extramedullary disease. Most were treated for acute myeloid leukemia (AML; n = 15), followed by acute lymphocytic leukemia (ALL; n = 9), non-Hodgkin lymphoma (NHL; n = 6), and multiple myeloma (MM; n = 4).

Of these patients, 18 received ACT and 16 were treated with CBT because of the absence of HLA-matched donors in a clinically useful time frame. Procedures for ACT and CBT asseverated previously described protocols.[18,19] Patients' characteristics are shown in Tables 1 and 2. The treatment plan was reviewed and approved by the local Ethics Committee, and written informed consent was obtained from all patients before any treatment, in accordance with the Declaration of Helsinki.

As requested by our standard operative treatments, myeloablative conditioning regimen and prophylaxis of graft-versus-host disease were accomplished by the conventional integrated approach. Briefly, all patients received fractionated 10 to 12 Gy total body irradiation on days −6, −5, and −4 before transplantation, plus thiotepa (8 mg/kg) on day −8; treosulfan (10-12 g/m^2 daily) on days −7, −6, and −5; fludarabine (40 mg/m^2 per day) from days −7 to −3; and cyclophosphamide (60 mg/kg per day) on days −2 and −1. IV cyclosporin was started on day −7 at a daily dose of 1 mg/kg and tapered from day +90 to day +180 after transplantation. Mycophenolate mofetil was given at a dose of 15 mg/kg orally twice daily in the first 28 days, and antithymocyte globulin was administered on days −3 and −2 (3 mg/kg). No patient received steroids. All patients received G-CSF.

HSC injection was performed via the IV route in all patients who underwent ACT, whereas patients who submitted to CBT received HSC administration via the intrabone route (4 injections and ~10^7 nucleated cells per kg of body weight).

Peripheral blood cell counts were estimated daily for the first month after transplant and twice weekly thereafter to estimate the median time of successful engraftment, defined as neutrophils >0.5 × 10^9/L and platelets >20 × 10^9/L for 3 consecutive days, respectively.[18]

Imaging data in transplanted patients were compared with corresponding findings in 34 age- and sex-matched controls, randomly selected from our normalcy database, represented by individuals who submitted to PET/CT as a long-term control of a completely excised, first-grade melanoma, with negative subsequent radiologic and clinical long-term follow-up for at least 2 years.[10]

PET/CT acquisition and reconstruction

After a minimum of 12 hours fasting, serum glucose was assessed to ensure a glucose level ≤1 g/L. Weight and height of all patients were measured. The

Table 2. Characteristics of patients treated with ACT

Patient	Gender	Age	Diagnosis	Platelets ($\times 10^9$/L)			Neutrophils ($\times 10^9$/L)			Axial ABM volume (ml/kg IBW)	Appendicular ABM volume (ml/kg IBW)	Disease status
				Day 30	Day 60	Day 100	Day 30	Day 60	Day 100			
1	M	50	AML	203	116	141	4.3	6	4.2	5.19	0.56	CR
2	M	55	AML	64	121	202	5.2	1.33	3.7	6.82	2.84	CR
3	M	21	NHL	122	135	143	3	2.4	4.1	6.61	2.30	SD
4	M	63	AML	141	167	180	3	2.4	5.2	4.79	5.68	SD
5	M	17	ALL	131	154	168	3.7	5.2	4.3	3.62	0.84	CR
6	M	34	ALL	255	239	289	8.6	8	6.3	4.27	10.13	CR
7	M	52	NHL	135	183	195	5.9	8	14.7	4.06	2.34	CR
8	F	52	MM	43	159	126	1.88	4.2	5.3	3.16	2.02	CR
9	M	65	ALL	127	88	28	4.1	5.46	8.5	5.52	2.68	CR
10	F	28	ALL	48	40	70	4.2	3.6	7.5	5.92	1.62	CR
11	F	60	NHL	207	250	296	3	2.9	2.7	5.98	0.15	CR
12	F	20	AML	236	209	228	5.8	4.8	3.7	6.47	0.37	PD
13	F	26	AML	65	161	194	1.9	1.9	2.8	5.91	0.53	CR
14	M	51	AML	136	103	135	0.47	5.1	3.7	3.93	0.67	CR
15	M	21	ALL	106	117	110	2.6	2.2	3.2	0.34	0.53	CR
16	M	25	NHL	58	84	161	2.6	1.3	4.1	4.61	0.89	CR
17	F	39	MM	183	244	244	1.7	1.9	2.3	3.66	2.43	CR
18	M	25	AML	127	156	181	2	2.5	4.9	5.68	1.72	CR
Mean		40 ± 17		133 ± 64	151 ± 58	172 ± 69	3.6 ± 1.9	3.8 ± 2.1	5.1 ± 2.9	4.8 ± 1.6	2.1 ± 2.4	15/18 CR
P vs CBT		NS		<.01	<.05	<.05	<.05	NS	NS	NS	<.05	NS

PD, progressive disease; SD, stable disease.

latter variable was used to calculate ideal body weight (IBW) according to the formulation of Robinson et al.20 A bolus injection of FDG was then performed (4.8-5.2 MBq/kg of body weight) while patients were lying in supine position in a quiet room and instructed not to move or talk. PET imaging started 60 to 75 minutes after tracer administration and was performed in three-dimensional (3D) mode, using an integrated PET/CT scanner (Hirez; Siemens Medical Solutions, Knoxville, TN). The whole body was scanned from vertex to toes in an "arms down" position. PET raw data were reconstructed by means of ordered subset expectation maximization (3 iterations, 16 subsets), and attenuation correction was performed using CT data. The transaxial field of view and pixel size of the reconstructed PET images were 58.5 cm and 4.57 mm, respectively, with a matrix size of 128 × 128. As per standard PET/CT imaging protocol, a 16-detector row helical CT scan was performed with nondiagnostic current and voltage settings, with a gantry rotation speed of 0.5 seconds and table speed of 24 mm per gantry rotation. No contrast medium was injected. The entire CT data set was fused with the 3D PET images using an integrated software interface (Syngo; Siemens Erlangen, Germany).

Image analysis

Image analysis was performed according to the previously validated method.[10] The algorithm identifies the skeleton on CT images by assuming that compact bone is the structure with the highest radiograph attenuation coefficient in the human body. Once it has identified the skeletal border, the program starts the thresholding algorithm, which samples a 2-voxel-thick layer and computes its average Hounsfield value. Thereafter, all skeletal voxels having attenuation coefficient equal or above this value are considered as compact bone, and the remaining as trabecular bone. The software output is the extraction and 3D representation of 3 different volumes: skeletal volume (SV), compact bone volume, and trabecular bone volume (IBV).

IBV is then voxel-wise multiplied against the PET coregistered data to extract and represent BM metabolic activity. The skull is intentionally excluded from the analysis because brain radioactivity spillover prevents an accurate assessment of IBV FDG uptake in this region. For the purposes of the present study, the computation of whole SVs was completed by a further segmental analysis: vertebrae and sternum accounted for the axial skeleton; humeral, femoral, and tibial/fibular shafts accounted for the appendicular skeleton.

All volumetric data were normalized for IBW. All IBV voxels were subdivided into active or inactive BM according to previously published statistical standards.[10] This criterion assumes that lumbar and thoracic vertebrae are almost fully occupied by ABM in normal subjects. In this district, average standardized uptake value (SUV) was found to be 2.01 ± 0.36 in a population of 102 normal subjects.[10] Assuming a normal distribution of these values, ABM was deemed to occupy all IBV voxels with SUV ≥1.11 (ie, mean − 2.5 standard deviations below the normal lumbar IBV average); on the other hand, all IBV voxels with tracer uptake index below this cutoff were considered as idle, fatty BM.

Statistical analysis

All data are reported as mean ± standard deviation. Unpaired or paired Student *t* tests were used to compare data in different groups or in the same group, as appropriate. The χ^2 test was used to verify difference in categorical variables. A *P* value <.05 was considered statistically significant. All statistical analyses were carried out using SPSS software version 23 (SPSS Inc., Chicago, IL).

Results

Clinical parameters

As shown in Tables 1 and 2, age, gender, and baseline characteristics were comparable in patients treated with ACT or CBT. At the evaluation time of PET, 15 out of 16 (93.8%) and 15 out of 18 (83%) patients showed a CR in the CBT and ACT group, respectively (Tables 1 and 2; *P* = NS).

As expected, ACT was associated with a faster recovery with respect to CBT: at day 30, platelet counts reached the cutoff value of 20 × 10^9/L in 15/18 (83%) of patients treated with ACT and only in 4/16 (25%) patients who submitted to CBT (*P* < .01; Figure 1 and Tables 1 and 2). This difference was confirmed by the fact that average platelet counts showed divergent values in the populations at all time points, as reported in Tables 1 and 2 and in Figure 1. Notably, however, at the latest observation (day 100), only 1 patient in the entire population

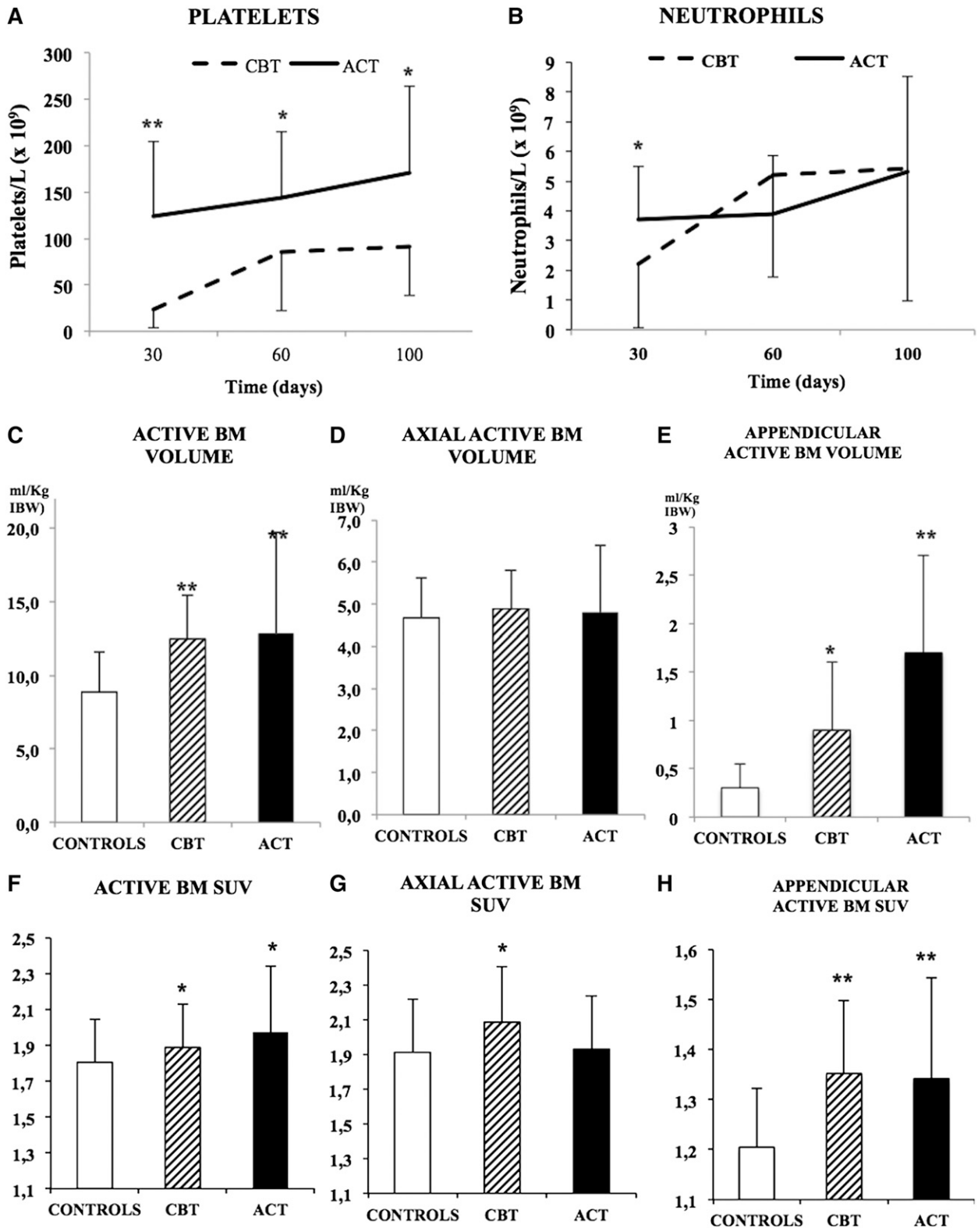

Figure 1. Posttransplant ABM distribution and hematopoietic recovery. The trend of platelet (A) and neutrophils (B) recovery at days 30, 60, and 100 in the ACT and CBT groups shows a better outcome in patients treated with adult HSCs. Normalized ABM volumes (C) show a significant expansion of hematopoietic tissue within the appendicular skeleton (E), whereas the axial compartment was unchanged (D). Glucose metabolism was increased in both ACT and CBT (F) with a relative increase in the axial skeleton of patients treated with CBT (G) and a marked increase in the appendicular skeleton of both groups (H). Statistical significance is represented as follows: *$P < .05$; **$P < .01$.

showed platelet numbers lower than the recovery threshold. Neutrophils counts showed a slightly different trend: values $>0.5 \times 10^9$/L occurred at day 30 in 17/18 (94%) and in 13/16 (81%) of patients in the ACT or CBT group ($P < .01$). As shown in Tables 1 and 2 and in Figure 1, their average counts diverged at first evaluation, whereas they became comparable at later time points.

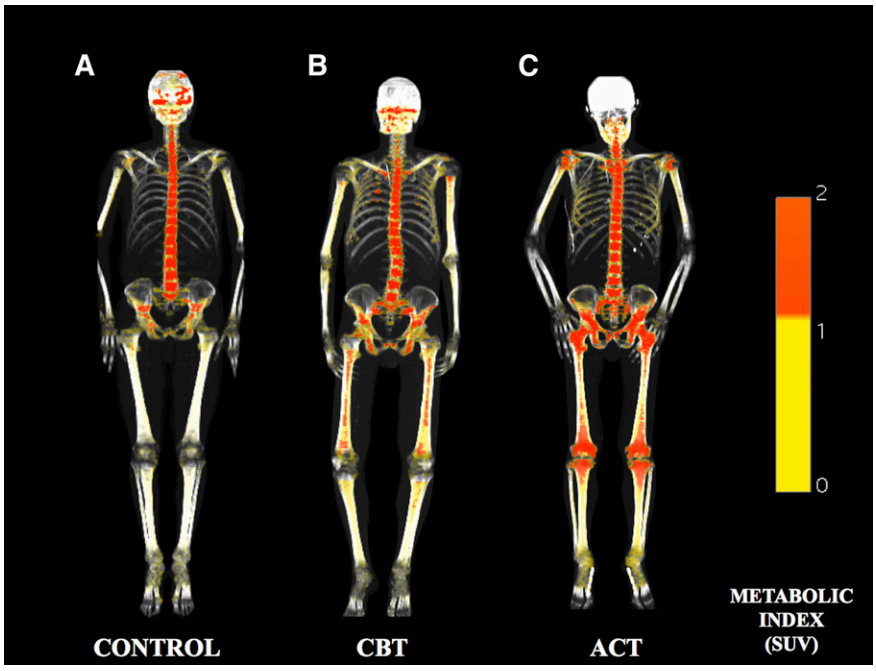

Figure 2. The 3D reconstructions of sample patients generated by the fusion of the automatically segmented FDG PET and CT data. Control subject (A) shows prevalent activity in the axial skeleton, whereas a patient treated with CBT (B) shows increased activity also in the hip bones and in the long bone shafts. (C) A patient treated with ACT shows a markedly increased glycolytic activity, extending up to the distal tibial epiphyses.

ABM distribution and metabolism

Throughout the whole skeleton, both CBT and ACT similarly expanded hematopoietic tissue. In fact, ABM volume was 12.4 ± 3 and 12.8 ± 6.8 mL/kg IBW after CBT and ACT, respectively, and it was significantly increased when compared with control subjects (8.1 ± 2.6 mL/kg IBW, $P < .001$). On the contrary, overall metabolic activity was only slightly, although significantly, augmented by transplantation, as ABM showed similar SUV in patients treated with CBT (1.96 ± 0.39) or ACT (1.96 ± 0.39), and both values were moderately increased with respect to control subjects (1.8 ± 0.2, $P < .05$) (Figure 1).

Intriguingly, the most impressive finding after both types of transplantation was a marked increase in ABM volume within the appendicular skeleton. This pattern was relatively more pronounced for ACT that occupied a larger volume of appendicular intraosseous space with respect to CBT (26 ± 27% vs 12 ± 11%, $P < .05$). Both data were significantly greater with respect to control values (5 ± 6%, $P < .001$ vs both transplant groups). Overall, appendicular ABM showed a sixfold expansion in ACT group with respect to controls (1.7 ± 1 vs 0.3 ± 0.2 mL/kg IBW, $P < .001$), whereas the increase was threefold in the CBT group (0.9 ± 0.6 mL/kg IBW, respectively, $P < .01$ vs controls; Figures 1 and 2).

On the other hand, metabolic activity (measured as SUV) of ABM within the appendicular skeleton was similarly augmented in both CBT and ACT (1.4 ± 0.1 and 1.3 ± 0.2, respectively, P = NS). These values were significantly higher than those observed in control subjects (1.2 ± 0.1, $P < .01$).

As previously reported, the axial skeleton was almost fully occupied by ABM in control subjects (88.5 ± 9.2% of IBV). In this setting, no significant variations were observed in either transplant modality (91.1 ± 5.2% and 89.8 ± 8.2% of IBV for CBT and ACT, respectively, P = NS). Similarly, metabolic activity of hematopoietic tissue was almost unchanged with the only exception of CBT that slightly increased axial BM SUV with respect to controls (2.1 ± 0.3 vs 1.9 ± 0.3, $P < .05$), whereas this variable remained unchanged in the ACT group (1.9 ± 0.3, P = NS vs controls).

Finally, disease status had no influence on ABM volumetric parameters: active volume, both in the axial and appendicular skeleton, was not significantly different between responders and nonresponders in both CBT and ACT groups.

Skeletal structure volumetric data in the patient cohort

Total SV was similar in patients treated with either CBT (81 ± 13.32 mL/kg IBW) or ACT (80.85 ± 12 mL/kg IBW), being close to the value observed in control subjects (86.6 ± 24.4 mL/kg IBW, P = NS vs both patients groups). However, transplanted patients displayed a remarkable skeletal alteration that was appreciated even at the visual inspection of CT slices, where the cortical bone was notably rarefied and the diameter of the bone canal was enlarged (Figure 3).

Indeed, compact bone volume was markedly eroded in all patients, both in CBT and ACT groups. This finding was attested to by absolute IBV volume as well as by the increased ratio between IBV and SV (40 ± 4% and 40 ± 7% vs 29 ± 5%, for CBT, ACT, and controls, respectively, $P < .001$) (Figure 3).

Interestingly, this alteration was almost undetectable in axial bone segments, whereas it was evident in long bone shafts where the ratio between medullary cavity and compact bone virtually doubled with respect to the control population (41 ± 4% and 42 ± 9% vs 18 ± 5% for CBT, ACT, and controls, respectively, $P < .001$; Figure 3).

Discussion

To the best of our knowledge, this study represents the first evidence of a peculiar distribution of transplanted BM cells in adult patients. Regardless of its source, transplanted BM showed intense glucose consumption in long bone shafts, which in normal adults are usually occupied by metabolically inert tissues.[1,10,13]

These findings suggest that in the setting of allogeneic BM transplantation, volumetric and metabolic parameters of ABM are regulated by at least partially different homeostatic pathways. Furthermore, volumetric expansion could be a key feature to meet the hugely increased hematopoietic workload and to achieve the reconstitution of the hematopoietic system in the shortest possible time.

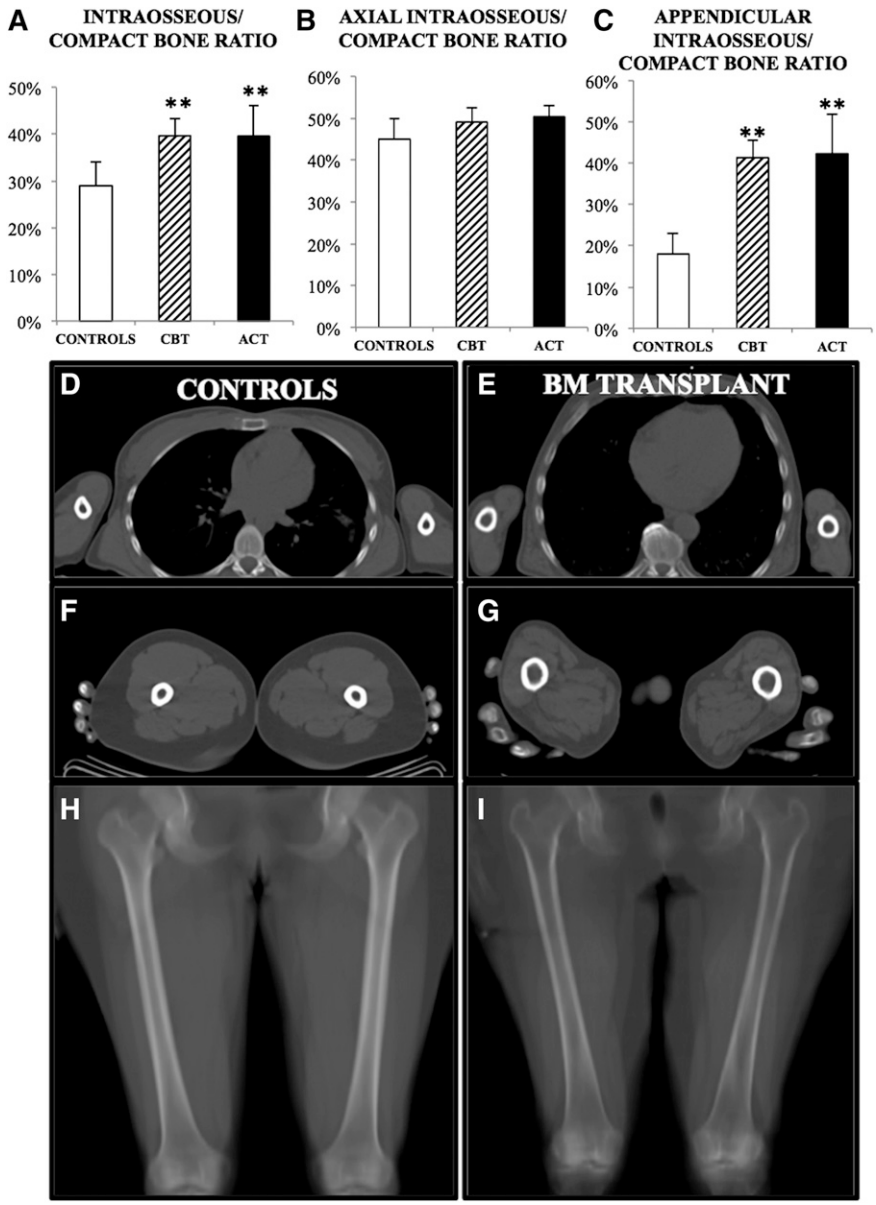

Figure 3. Structural alterations in patients with hematologic conditions. In both patient groups, cortical bone erosion was present, causing a significant increase in the ratio between intraosseous space and total SV (A). This difference was largely caused by marked erosion in the appendicular district (C), whereas the axial skeleton was unmodified (B). (D-G) Transaxial slices of a transplanted patient (E, G), showing visible cortical erosion, as compared with a matched control (D, F). (H-I) Mean intensity projections of a coronal slice of femurs, showing marked erosion in the transplanted patient (I), compared with control (H). Significance was represented as follows: $*P < .05$; $**P < .01$.

BM metabolism and BM transplant

After its introduction in clinical oncology, FDG PET/CT became a major tool to evaluate chemotherapy effectiveness. In several previous studies, serial monitoring of FDG uptake documented that autochthonous BM regeneration after myelotoxic agents is confined to axial skeletal segments and implies a substantial increase in FDG uptake.[21-25] This response did not occur after allogeneic transplant, as axial segments showed values that were comparable to the ones of control subjects and the marked increase of metabolic activity documented the colonization of appendicular areas.

The divergent BM responses to transplantation and chemotherapy suggest the presence of different regulating mechanisms. In this line, the additional, appendicular bone colonization seems to be a peculiar feature of allotransplanted HSCs. Obviously, the peculiar distribution pattern after transplantation might have been influenced by the accelerated proliferation, maturation, and mobilization of HSCs induced by G-CSF, which is commonly used, both after transplant and chemotherapy, to reduce the time of neutrophil recovery.[4] However, G-CSF does not produce colonization of appendicular bones during BM regeneration after chemotherapy.[21-25] Thus, we can conclude that the colonization of abandoned BM areas is a "unique feature" of allotransplant and is independent of both administration route (intrabone or IV) and hematopoietic source (cord blood or adult BM).

We found that ACT occupied long bone shafts with higher efficiency with respect to CBT. The difference in appendicular bone colonization between ACT vs CBT might explain, at least in part, the difference in the recovery speed of peripheral blood parameters. Of course, with our technique we cannot document whether there is a skewed representation of individual clones in different bone, as described in the preclinical setting.[4] However, why allogeneic transplanted cells prefer not to "force" cell proliferation in previously active niches but favor to "delocalize" the production of hematopoietic cells in appendicular skeleton may hide an important regulatory mechanism and warrants further investigation. Finally, it is noteworthy that cord blood cells are able to recolonize (at 30 days after CBT) the BM spaces nearly to the same extension with respect

to ACT. This observation suggests that the high proliferative potential of cord blood–derived HSCs considerably smoothed the 10-fold difference in the hematopoietic cell number of the graft.[26]

Skeletal structure in BM transplant recipients

Our computational approach documented a significant reduction in compact bone thickness, mostly evident in the appendicular skeleton. This finding was somewhat expected, on the basis of previous experimental, biological, and radiologic studies, reporting an altered skeletal structure in the presence of leukemia or myeloma.[27-29] The mechanisms underlying this alteration are largely unknown; however, this finding indicates that disease consequences extend to the whole skeleton, including skeletal segments that are remote from the localization of neoplastic burden. These data confirm the relevant impact of aggressive hematologic malignancies on skeletal structure. In this line, the availability of imaging approaches to the skeletal composition might complement the overall disease characterization, improving our understanding of the neoplasia-bone interactions.

Limitations

Several limitations of the present study have to be carefully considered. First, study patients were submitted to BM transplantation for different hematologic conditions. This variability might imply a heterogeneous alteration in bone structure and in BM space occupancy by transplanted cells. Although, colonization of long bone shafts was observed in virtually all patients, the mechanisms underlying this variability (most likely related to physiological factors, preexisting disease, and transplanted HSC characteristics) cannot be defined on the basis of the present study.

On a technical ground, pertaining the partial volume effect occurring when employing low-current CT settings and potentially causing errors in estimating the intraosseous volume, due to the reduced capability of these CT settings to detect the bone trabeculae, has already been raised.[10,29] However, previous studies have shown that the figures produced by our software are operator independent and reproducible and that they match, at least in the regional evaluation, current imaging standards.[30]

Conclusions

In summary, these data indicate that allogeneic transplantation of either adult or cord blood HSCs colonize not only the areas of physiological residency of BM but also the appendicular skeleton that, in adult healthy subjects, is not a site of active hematopoiesis any more. This also implies that some hematopoietic niches are rebuilt and /or rejuvenated, in order to restore hematopoiesis.

Understanding the pathophysiology of this response will help in defining the nature of mechanisms governing BM extension in adulthood and could stimulate further and newer approaches in order to better understand the mechanisms regulating homing and colonization of transplanted HSCs.

Acknowledgments

This work was supported by the Progetto regionale per ricerca sanitaria, "Studying the trafficking of stem cells, mesenchymal stem cells and endothelial cells as a tool to improve transplant effectiveness"; Ricerca Corrente 5XMILLE to Istituti di Ricovero e Cura e Carattere Scientifico San Martino Istituto Scientifico Tumori from Italian Ministry of Health; Ricerca Corrente 5XMILLE 2012-13 to Istituto Giannina Gaslini from Italian Ministry of Health; Compagnia di San Paolo 2014 AAI637.U/812/AR pv 2013.0958 (F. Frassoni); and the CNR-IBFM project: "Cell-based Omics for Biomedical Research Applications."

Authorship

Contribution: F. Fiz, C.M., G.S., A.B., M. Piana, M. Podestà, and F. Frassoni devised the rationale and designed the study protocol; F. Fiz, G.B., R.P., G.S., M.Piana, M. Podestà, F. Frassoni, and F.B. performed the data analysis and interpretation; C.C., A.M.M., and M. Piana designed the software application and performed the mathematical/statistical analysis; all authors participated in manuscript writing, editing, and revision; and all authors have read and approved the final version of the manuscript.

Conflict-of-interest disclosure: The authors declare no competing financial interests.

Correspondence: Francesco Frassoni, Department of Pediatric Hemato-Oncology, Stem Cell and Cell Therapy Laboratory, Istituto G. Gaslini, Genoa, Italy, Largo G. Gaslini, 5, 16147 Genoa, Italy; e-mail: francesco.l.frassoni@gmail.com.

References

1. Hayman JA, Callahan JW, Herschtal A, et al. Distribution of proliferating bone marrow in adult cancer patients determined using FLT-PET imaging. *Int J Radiat Oncol Biol Phys.* 2011;79(3): 847-852.
2. Bhojwani D, Howard SC, Pui CH. High-risk childhood acute lymphoblastic leukemia. *Clin Lymphoma Myeloma.* 2009;9(suppl 3): S222-S230.
3. Uchida N, Aguila HL, Fleming WH, Jerabek L, Weissman IL. Rapid and sustained hematopoietic recovery in lethally irradiated mice transplanted with purified Thy-1.1lo Lin-Sca-1+ hematopoietic stem cells. *Blood.* 1994;83(12):3758-3779.
4. Verovskaya E, Broekhuis MJ, Zwart E, et al. Asymmetry in skeletal distribution of mouse hematopoietic stem cell clones and their equilibration by mobilizing cytokines. *J Exp Med.* 2014;211(3):487-497.
5. Shehee WR, Oliver P, Smithies O. Lethal thalassemia after insertional disruption of the mouse major adult beta-globin gene. *Proc Natl Acad Sci USA.* 1993;90(8):3177-3181.
6. Koury MJ. Abnormal erythropoiesis and the pathophysiology of chronic anemia. *Blood Rev.* 2014;28(2):49-66.
7. Ting-Beall HP, Needham D, Hochmuth RM. Volume and osmotic properties of human neutrophils. *Blood.* 1993;81(10):2774-2780.
8. McLaren CE, Brittenham GM, Hasselblad V. Statistical and graphical evaluation of erythrocyte volume distributions. *Am J Physiol.* 1987; 252(4, pt 2):H857-H866.
9. Podesta M, Piaggio G, Frassoni F, et al. The assessment of the hematopoietic reservoir after immunosuppressive therapy or bone marrow transplantation in severe aplastic anemia. *Blood.* 1998;91(6):1959-1965.
10. Sambuceti G, Brignone M, Marini C, et al. Estimating the whole bone-marrow asset in humans by a computational approach to integrated PET/CT imaging. *Eur J Nucl Med Mol Imaging.* 2012;39(8):1326-1338.
11. Iscove NN, Nawa K. Hematopoietic stem cells expand during serial transplantation in vivo without apparent exhaustion. *Curr Biol.* 1997; 7(10):805-808.
12. Aoki J, Ohashi K, Mitsuhashi M, et al. Posttransplantation bone marrow assessment by quantifying hematopoietic cell-derived mRNAs in plasma exosomes/microvesicles. *Clin Chem.* 2014;60(4):675-682.
13. Cristy M. Active bone marrow distribution as a function of age in humans. *Phys Med Biol.* 1981; 26(3):389-400.
14. Yao WJ, Hoh CK, Hawkins RA, et al. Quantitative PET imaging of bone marrow glucose metabolic

response to hematopoietic cytokines. *J Nucl Med.* 1995;36(5):794-799.

15. Knopp MV, Bischoff H, Rimac A, Oberdorfer F, van Kaick G. Bone marrow uptake of fluorine-18-fluorodeoxyglucose following treatment with hematopoietic growth factors: initial evaluation. *Nucl Med Biol.* 1996;23(6):845-849.
16. Sugawara Y, Fisher SJ, Zasadny KR, Kison PV, Baker LH, Wahl RL. Preclinical and clinical studies of bone marrow uptake of fluorine-1-fluorodeoxyglucose with or without granulocyte colony-stimulating factor during chemotherapy. *J Clin Oncol.* 1998;16(1):173-180.
17. Murata Y, Kubota K, Yukihiro M, Ito K, Watanabe H, Shibuya H. Correlations between 18F-FDG uptake by bone marrow and hematological parameters: measurements by PET/CT. *Nucl Med Biol.* 2006;33(8):999-1004.
18. Frassoni F, Gualandi F, Podestà M, et al. Direct intrabone transplant of unrelated cord-blood cells in acute leukaemia: a phase I/II study. *Lancet Oncol.* 2008;9(9):831-839.
19. Copelan EA. Hematopoietic stem-cell transplantation. *N Engl J Med.* 2006;354(17):1813-1826.
20. Robinson JD, Lupkiewicz SM, Palenik L, Lopez LM, Ariet M. Determination of ideal body weight for drug dosage calculations. *Am J Hosp Pharm.* 1983;40(6):1016-1019.
21. Avivi I, Zilberlicht A, Dann EJ, et al. Strikingly high false positivity of surveillance FDG-PET/CT scanning among patients with diffuse large cell lymphoma in the rituximab era. *Am J Hematol.* 2013;88(5):400-405.
22. Tang B, Patel MM, Wong RH, et al. Revisiting the marrow metabolic changes after chemotherapy in lymphoma: a step towards personalized care. *Int J Mol Imaging.* 2011;2011:942063.
23. Ulaner GA, Lyall A. Identifying and distinguishing treatment effects and complications from malignancy at FDG PET/CT. *Radiographics.* 2013;33(6):1817-1834.
24. Rose BS, Liang Y, Lau SK, et al. Correlation between radiation dose to ^{18}F-FDG-PET defined active bone marrow subregions and acute hematologic toxicity in cervical cancer patients treated with chemoradiotherapy. *Int J Radiat Oncol Biol Phys.* 2012;83(4):1185-1191.
25. Park S, Lee SJ, Chang WJ, et al. Positive correlation between baseline PET or PET/CT findings and clinical parameters in multiple myeloma patients. *Acta Haematol.* 2014;131(4):193-199.
26. Frassoni F, Podesta M, Maccario R, et al. Cord blood transplantation provides better reconstitution of hematopoietic reservoir compared with bone marrow transplantation. *Blood.* 2003;102(3):1138-1141.
27. Frisch BJ, Ashton JM, Xing L, Becker MW, Jordan CT, Calvi LM. Functional inhibition of osteoblastic cells in an in vivo mouse model of myeloid leukemia. *Blood.* 2012;119(2):540-550.
28. Secchiero P, Corallini F, Barbarotto E, et al. Role of the RANKL/RANK system in the induction of interleukin-8 (IL-8) in B chronic lymphocytic leukemia (B-CLL) cells. *J Cell Physiol.* 2006;207(1):158-164.
29. Fiz F, Marini C, Piva R, et al. Adult advanced chronic lymphocytic leukemia: computational analysis of whole-body CT documents a bone structure alteration. *Radiology.* 2014;271(3):805-813.
30. Basu S, Houseni M, Bural G, et al. Magnetic resonance imaging based bone marrow segmentation for quantitative calculation of pure red marrow metabolism using 2-deoxy-2-[F-18] fluoro-D-glucose-positron emission tomography: a novel application with significant implications for combined structure-function approach. *Mol Imaging Biol.* 2007;9(6):361-365.

2015 125: 4095-4102
doi:10.1182/blood-2015-01-618215 originally published online May 8, 2015

Allogeneic cell transplant expands bone marrow distribution by colonizing previously abandoned areas: an FDG PET/CT analysis

Francesco Fiz, Cecilia Marini, Cristina Campi, Anna Maria Massone, Marina Podestà, Gianluca Bottoni, Roberta Piva, Francesca Bongioanni, Andrea Bacigalupo, Michele Piana, Gianmario Sambuceti and Francesco Frassoni

Blood (print ISSN 0006-4971, online ISSN 1528-0020), is published weekly by the American Society of Hematology, 2021 L St, NW, Suite 900, Washington DC 20036.